Soft Magnetic Properties of Magnetic Cores Assembled With a High B_s Fe-Based Nanocrystalline Alloy

Motoki Ohta[1] and Ryusuke Hasegawa[2]

[1]Metallurgical Research Laboratory, Hitachi Metals Ltd., Yasugi 692-8601, Japan
[2]Metglas Inc., Conway, SC 29526 USA

Soft magnetic properties of magnetic cores assembled with $Fe_{81.8}Cu_{1.0}Mo_{0.2}Si_4B_{14}$ nanocrystalline alloy ribbon are discussed. The nanocrystalline alloy ribbon was cast in an amorphous phase by a melt quenching method, and a nanocrystalline phase was obtained by high-heating rate annealing. A medium-size toroidal core assembled with this nanocrystalline alloy ribbon exhibits magnetic flux density B_{800} at 800 A/m of 1.74 T, core loss $P_{16/50}$ at 50 Hz, and at 1.5 T of 0.29 W/kg. A racetrack-shaped core, which includes curved and straight sections in the same core, exhibits core losses at 1.0 T and at 400 Hz and 1 kHz of 1.5 and 5 W/kg, respectively. These core losses are as low as those of Fe-based amorphous alloys. A medium-size toroidal core assembled with this nanocrystalline alloy ribbon, secondarily annealed under a perpendicular magnetic field, exhibits core loss $P_{2/10k}$ at 0.2 T and at 10 kHz of 2 W/kg. This value of core loss is one of the lowest values for the metallic magnetic cores, which have a saturation induction B_s higher than 1.5 T. A core assembled with this material can be used in several applications from low to medium frequency ranges. Since this material exhibits a higher B_s and one half of the saturation magnetostriction λs of Fe-based amorphous alloys with comparable core losses, the most possible applications are in such applications as distribution transformers and inductors in power electronics.

Index Terms— **High B_s soft magnetic materials, nanocrystalline magnetic materials, toroidal core.**

I. Introduction

CURRENTLY, soft magnetic materials, such as Si-steels [1]–[4], Fe-based amorphous alloys [5]–[7], and Fe-based nanocrystalline alloys [8]–[10], are used in electrical power devices and modern electronics equipment, parts, and devices, which require high efficiency. Especially for low frequency applications such as distribution transformers, a high operating magnetic flux density B_m with low core loss is required for the core material to achieve high effectiveness. In this application field, grain-oriented Si-steels have been most widely used. However, Fe-based amorphous alloys are increasingly replacing Si-steels because of their lower core loss [7]. Comparing these two materials, there is a tradeoff relation between B_m and core loss. Since saturation flux densities B_s of Fe-based amorphous alloys are at most approximately 1.65 T, which is about 80% of that of oriented Si-steels [11], a transformer made by an Fe-based amorphous alloy is 1.1 $\sim$ 1.2 times larger than that made by Si-steels. Therefore, a combination of high B_s and low core loss is required for the next generation of soft magnetic materials for transformers. From this point of view, high B_s Fe-Cu-B and Fe-Cu-Si-B nanocrystalline alloys have been developed, which exhibit B_s of higher than 1.7 T and core loss at 50 Hz and at 1.5 T, $P_{15/50}$, of one half of that of grain oriented Si-steels [12]–[18]. These materials were cast as ribbon by a melt quenching method and nanocrystalline phases were obtained after annealing. The as-quenched state exhibited primary crystalline grains of sizes of several nanometers with number density of more than 500 grains/μm^2 in the matrix of Fe-B-based amorphous phase [7]. Because of this alloy ribbon being brittle in the as-quenched state, there are issues of ribbon-winding during the continuous casting process. It was difficult to obtain consistent ribbon at the production level. Therefore, high B_s Fe-Nb-Cu-Si-B and Fe-Cu-Si-B-P nanocrystalline alloys, which exhibit B_s of higher than 1.7 T and core loss, for example, at 50 Hz and at 1.5 T, $P_{15/50}$, of one third of that of oriented Si-steels, have been developed [15]–[17]. These alloys can be cast in amorphous phases. However, in order to obtain nanocrystalline phases, they required high heating rate of more than 100 °C/min in the annealing process [15], [16]. To achieve this high heating rate, less than 20 sheets of strips were wrapped by thin Nb foil and were placed in a pre-heated furnace. No issues were found in annealing fewer than 20 sheets at the same time, but annealing more than 30 sheets at the same time tended to be uncontrollable. Due to the latent heat of crystallization, the ribbon is self-heated during the annealing process and ribbon stacking density is limited. Therefore, even for a small toroidal core of the size of outside diameter (OD), inside diameter (ID), and core thickness t of 19, 15, and 5 mm, respectively, the coercivity H_c was several hundreds of A/m because of the precipitation of Fe-B compounds due to overheating of the core during the annealing process. In order to solve this issue, we have developed an in-line pre-annealing system to obtain primary crystalline grains before final annealing. In this paper, soft magnetic properties of magnetic cores assembled with the amorphous alloy ribbon developed are presented.

Manuscript received May 14, 2016; revised September 19, 2016; accepted October 18, 2016. Date of publication October 21, 2016; date of current version January 24, 2017. Corresponding author: M. Ohta (e-mail: motoki.ota.tw@hitachi-metals.com).

Color versions of one or more of the figures in this paper are available online at http://ieeexplore.ieee.org.

Digital Object Identifier 10.1109/TMAG.2016.2620118

II. Experiment

In this paper, the chemical composition of the alloy ribbon is $Fe_{81.8}Cu_1Mo_{0.2}Si_4B_{14}$. An alloy ingot was melted by

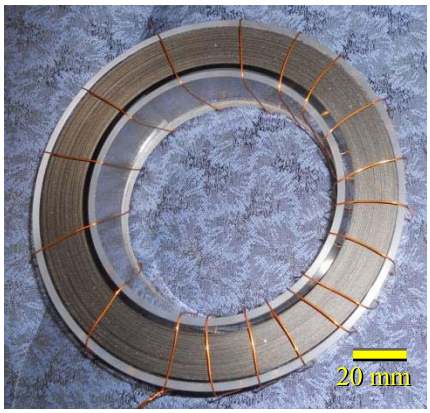

Fig. 1. Toroidal core of the size of ID117-OD153-t25.4 assembled with $Fe_{81.8}Cu_{1.0}Mo_{0.2}Si_4B_{14}$ nanocrystalline alloy ribbon. The weight of this core is approximately 1.2 kg. The nanocrystalline alloy ribbon was prepared by high speed heating rate anneal. After assembling the toroidal core, secondary annealing was carried out under a magnetic field of 2.2 kA/m applied along toroid's circumference direction.

induction heating in an Ar gas atmosphere. The ingot weighing about 20 kg is cast into 25.4 mm-wide amorphous ribbon with thicknesses of 23–25 μm by a melt quenching method. The crystallization temperatures T_{X1} and T_{X2} measured by DSC were approximately 480 °C and 530 °C, respectively. Here, T_{X1} and T_{X2} denote the precipitation temperature of bcc Fe and Fe–B compounds, respectively. The primary annealing was carried out by in-line annealing equipment. This equipment consists of a ribbon feeder hub, a tensionner, a heater, and a winder. The heater temperature was set at around 500 °C. Toroidal cores to be studied were directly assembled on the in-line annealing equipment. The average speed of heating from room temperature to the set temperature was higher than 100 °C/s. A typical secondary annealing condition was at 430 °C for 5.4 ks with a magnetic field of 2.2 kA/m applied along ribbon's length direction. The dc-magnetic measurements were performed by a commercially available dc-hysteresis loop tracer, Remagraph C-500 (manufactured by Magnet-Physik Dr. Steingroever, GmbH, Deutschland). Primary and secondary circuits were wound on the toroidal cores. The dc-hysteresis loops were measured by sweeping the magnetic field up to ±800 A/m. The ac-magnetic measurements were carried out according to ASTM A912 Standard using the same primary and secondary circuits prepared for dc-magnetic measurements. Sinusoidal excitations were adopted in the ac measurements, and the magnetic field was calculated by measuring the voltage across a shunt resistance. The microstructure was observed by a transmission electron microscopy (TEM).

III. Result and Discussion

A toroidal core with a size of (OD, ID, t) = (153, 117, 25.4 mm) is shown in Fig. 1. The weight of this core is approximately 1.2 kg. Since the natural radius of curvature of the primary in-line annealed ribbon is approximately 55 mm, the largest radius of curvature mismatching of the ribbon in the core is about 20 mm. Therefore, the core was secondarily annealed after assembling by a primary in-line annealing system in order to release the stress introduced during the

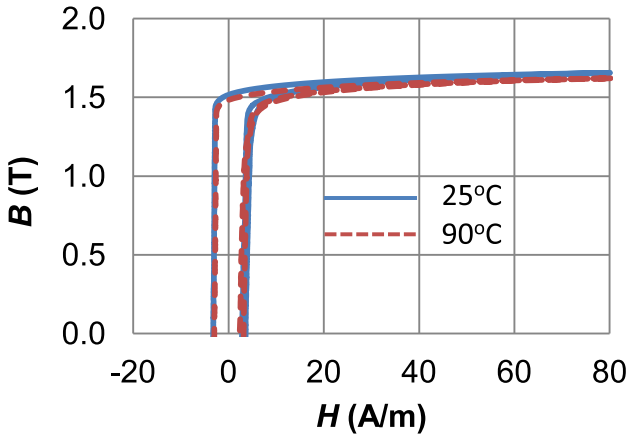

Fig. 2. B–H loop of the toroidal core of Fig. 1.

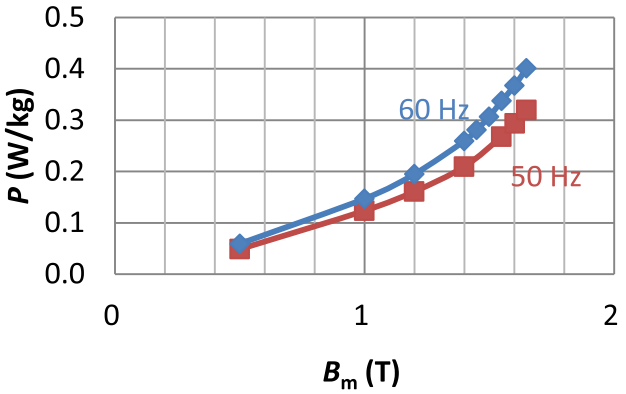

Fig. 3. Operating magnetic flux density B_m dependence of core loss P of the toroidal core of Fig. 1.

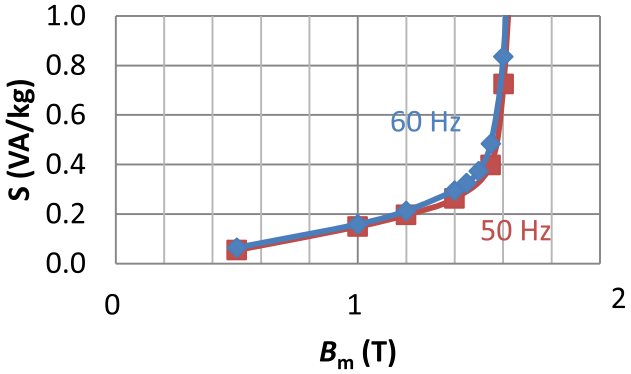

Fig. 4. Exciting power S of the toroidal core of Fig. 1 versus operating flux density B_m.

core assembling. Note that this secondary annealing serves mainly to release stress and to induce magnetic anisotropy under magnetic fields. By applying longitudinal magnetic fields along the magnetic pass direction (termed longitudinal field annealing below), the core could exhibit a square B–H loop. On the other hand, B–H loop could be a sheared-type by applying a magnetic field along the core's axis direction (termed "perpendicular field annealing" below). Moreover, the increase of B_s by secondary annealing is at most 0.02 T, hence most of the nanocrystallization has been completed during the primary annealing process. In Fig. 2,

TABLE I

VALUES OF B_{800}, B_{80}, $P_{15/50}$, AND $P_{16/50}$, AND B_s FOR A TOROIDAL CORE OF SIZE OF ID117-OD153-t 25.4 ASSEMBLED WITH $Fe_{81.8}Cu_{1.0}Mo_{0.2}Si_4B_{14}$ NANOCRYSTALLINE ALLOY RIBBON SHOWN IN FIG. 1 TOGETHER WITH THOSE VALUES FOR METGLAS®2605HB1m Fe-BASED AMORPHOUS ALLOY AND 230 μm THICK PLATE OF GRAIN ORIENTED Si-STEEL. ρ IS THE MATERIAL DENSITY

Material	Size (mm)	ρ (kg/dm^3)	B_{800} (T)	B_{80} (T)	$P_{15/50}$ (W/kg)	$P_{16/50}$ (W/kg)	B_s (T)
Nanocrystalline alloy	ID117-OD153-*t*25.4	7.42	1.74	1.66	0.24	0.29	1.75
Fe-Amorphous Metglas®2605HB1	ID116-OD153-*t*25.4	7.35	1.63	1.56	0.20	--	1.64
Grain Oriented Si-steel	230μm Plate	7.65	1.92	1.75	0.59	0.68	2.03

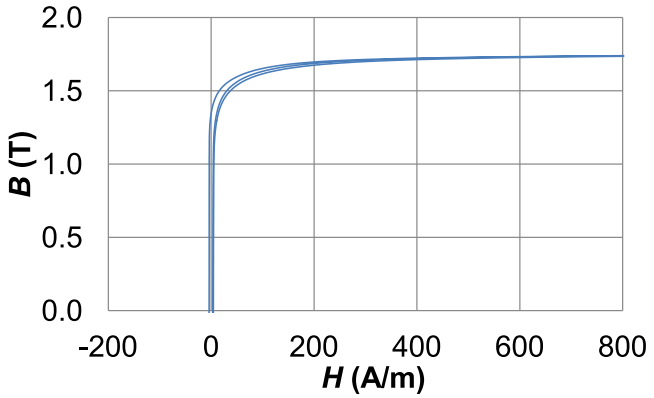

Fig. 5. B–H loop of a racetrack style core with a curved section with the radius of curvature of 30 mm and a straight section of 60 mm in length assembled with the primary annealed ribbon. Secondary anneal was performed under a longitudinal magnetic field.

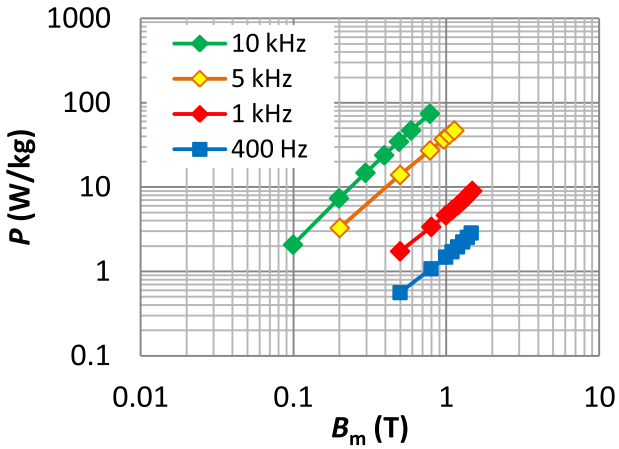

Fig. 6. Core loss P versus operating flux density B_m at frequencies of 400 Hz, and 1, 5, and 10 KHZ for the racetrack core Fig. 5.

B–H curves measured at 25 °C and 90 °C of this core are shown. Figs. 3 and 4, respectively, show power loss P versusB_m and exciting power S versus B_m measured at 25 °C. Representative data points from Figs. 2–4 are listed in TABLE I together with materials' saturation induction, B_s, and physical density, ρ. It is noted that the core loss of the present alloy is less than one half of that of Si-steels and comparable with that of the most advanced amorphous Fe-based alloy [18]. Also, noted are the ratios of B_{80}/B_s and B_{800}/B_samong the three materials: 0.95 and 0.99 for the present alloy and the amorphous alloy, respectively, whereas they are 0.86 and 0.95 for the Si-steel. These numbers indicate that B–H loops for the present alloy and the amorphous alloy are square in shape whereas the Si-steel loops are round, meaning B_m can be much closer to B_s, keeping the transformer's exciting power at much lower levels than in Si-steel-based transformers. As shown in Fig. 2, this core exhibits $B_{80} = 1.66$ T at 25 °C and 1.62 T at 90 °C, namely, the reduction ratio of B_{80} against temperature is −0.0006 T/°C. This is about one half of that of Fe-based amorphous alloys. Therefore, there is an advantage of a higher B_m for the present alloy over amorphous alloys with comparable core loss, providing highly balanced performance of B_m and loss in a transformer core based on the present alloy.

By using the same nanocrystalline ribbon, a racetrack-style core in which the curved section had a radius of curvature of 30 mm and a straight section of 60 mm was assembled. A secondary annealing was applied to this core. As shown in Fig. 5, this core exhibits a round B–H loop, indicating the magnetization process is by magnetization rotation whereas in the toroidal core of Fig. 1, domain wall motion is considered predominant in the magnetization process. In the racetrack core, there are higher stresses due to mismatching of ribbon curvatures. These stresses tend to divide magnetic domains, and hence finer and stiffer magnetic domains are created. This type of B–H loop is more suitable in higher frequency range of several kilohertzs. Core loss measurements were thus carried out at 400 Hz, and 1, 5, and 10 kHz, as shown in Fig. 6. The values of B_s, core losses of $P_{15/50}$ at 1.5 T and at 50 Hz, $P_{10/400}$ at 1.0 T and at 400 Hz, $P_{10/1k}$ at 1.0 T and at 1 kHz, and $P_{2/10k}$ at 0.2 T and at 10 kHz, and the saturation magnetostriction λ_s for this racetrack core are listed in TABLE II. Also listed are the data taken on a toroidal core with (OD, ID, t) = (74, 70, 25.4 mm) assembled with this material secondarily annealed under a perpendicular magnetic field and cores based on Metglas 2605HB1M Fe-based amorphous alloy, grain oriented Si-steel [18], 6.5 wt% Si-steel [19], and FINEMET FT3 Fe-based nanocrystalline alloy. The racetrack core exhibits comparable performance with Metglas 2605HB1M Fe-based amorphous alloy core in the 400 Hz ∼ 1 kHz range, showing an excellent performance at 10 kHz. The core with the

TABLE II

VALUES OF B_s, CORE LOSSES OF $P_{15/50}$ AT 1.5 T AND AT 50 Hz, $P_{10/400}$ AT 1.0 T AND AT 400 Hz, $P_{10/1k}$ AT 1 T AND AT 1 KHz AND $P_{2/10k}$ AT 0.2 T AND AT 10 KHz, AND THE SATURATION MAGNETOSTRICTION λ_s FOR THE RACETRACK CORE OF FIG. 5, COMPARING WITH THOSE DATA FOR id70-od74-t 25.4 TOROIDAL CORE ASSEMBLED WITH THE NANOCRYSTALLINE MATERIAL WITH A SECONDARY ANNEALING UNDER PERPENDICULAR MAGNETIC FIELD, METGLAS®2605HB1 Fe-BASED AMORPHOUS ALLOY CORE, GRAIN ORIENTED Si-STEEL, 6.5 wt% Si-STEEL, AND FINEMET®FT3 FE-BASED NANOCRYSTALLINE ALLOY CORE

	B_s (T)	$P_{15/50}$ (W/kg)	$P_{10/400}$ (W/kg)	$P_{10/1k}$ (W/kg)	$P_{2/10k}$ (W/kg)	λ_s (10^{-6})
Nanocrystalline alloy Racetrack Core	1.75	0.28	1.5	5	8	15
Nanocrystalline alloy Perpendicular field annealed	1.75	--	--	0.6	2	15
Metglas® 2605HB1 alloy	1.64	0.16	1.3	4.4	12	27
Grain Oriented Si-steel	2.03	0.59	7.8	27.1	--	7
6.5 wt%Si-steel	1.80	--	5.7	18.1	30	0
FINEMET® (FT3) alloy	1.25	--	--	--	< 2	0

perpendicular magnetic field annealing exhibits comparable core loss with that of FINEMET FT3 Fe-based nanocrystalline alloy core at 10 kHz.

In the medium frequencies, e.g., several kilohertz regions, the core loss determines the limit for B_m in transformers and other devices, unlike in lower-frequency transformers, because of the heat generated by core loss. From this point of view, FINEMET® FT3 Fe-based nanocrystalline alloy core is the most suitable metallic core for the transformers and inductors operated at B_m of less than 1.25 T. For power electronics applications, not only low core loss is required but also higher B_s values have to be considered as the inductors carrying large currents. A higher B_s results in smaller devices. Furthermore, lower core loss allows higher temperature operation. A loss separation analysis of the data obtained indicates that material hysteresis loss, eddy current loss, and excess eddy current are 0.8, 0.5 and 0.7 W/kg, respectively, at B_m of 0.2 T and at 10 kHz. It is possible to reduce core loss at higher frequencies by using thinner ribbons. In the frequency range above 20 kHz, eddy current loss becomes dominant; hence, suppressing eddy current by reducing inter-layer electrical conductivity is an efficient way to reduce core loss. In Fig. 7, cross-sectional TEM images near the ribbon facing the chill-roll surface of this material are shown. Crystalline grain sizes in the matrix phase of after annealed ribbon were $10 \sim 20$ nm. Note that the thickness of oxide layer on the as-quenched ribbon is 5 nm [shown in Fig. 7(a)], and it is $10 \sim 15$ nm after the primary annealing process [shown in Fig. 7(b)]. Although this core assembling method is less productive due to the requirement of two annealing steps with the primary step

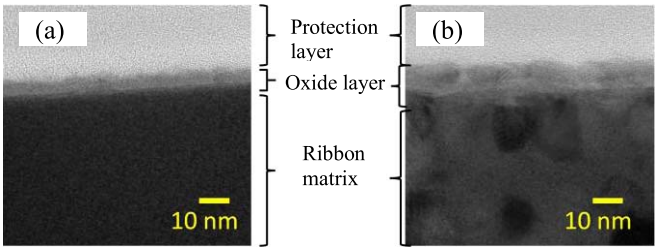

Fig. 7. Cross-sectional TEM image near roll surface side of (a) as-quenched and (b) annealed ribbon.

being by one-layer annealing, this process helps create a strong and homogeneous oxide layer on the surface of the ribbon. In fact, sticking of layers after secondary annealing was hardly observed for the cores assembled with this alloy ribbon. The sticking of layers brings about not only a high inter-layer electrical conductivity but also introduces local mechanical stress. Thus, the combination of the material and the annealing methods, i.e., the rapid annealing of $Fe_{81.8}Cu_{1.0}Mo_{0.2}Si_4B_{14}$ amorphous alloy ribbon, opens up a new opportunity of achieving highly efficient metallic magnetic cores in low- to medium-frequency applications. This material exhibits λ_s of around 15×10^{-6}, which is larger than those of Si-steels. However, λ_s is about one half of that of Fe-based amorphous alloy and this material exhibits a higher B_s and comparable core losses with Fe-based amorphous alloys. Thus, the inductors based on the present material emanate lower magnetostriction-related noises compared with those based on the amorphous Fe-based alloys, when operated at the same induction level.

IV. Conclusion

Soft magnetic properties of magnetic cores assembled with $Fe_{81.8}Cu_{1.0}Mo_{0.2}Si_4B_{14}$ nanocrystalline alloy ribbon are evaluated. The nanocrystalline alloy ribbon was cast in an amorphous phase by melt quenching method, and a nanocrystalline phase was obtained by rapid heating of the ribbon. The main conclusions are as follows.

A medium-sized toroidal core assembled with this nanocrystalline alloy ribbon exhibits magnetic flux density B_{800} at 800 A/m of 1.74 T and core loss $P_{16/50}$ at 50 Hz and at 1.5 T of 0.29 W/kg. The value of B_{800} is about 0.1 T higher than that of Fe-based amorphous alloys and $P_{16/50}$ is less than one half of that of grain oriented Si-steels.

A racetrack-shaped core, which includes curved and straight sections in the same core, exhibits core losses at 1.0 T and at 400 Hz and 1 kHz of 1.5 and 5 W/kg, respectively. Due to the mechanical stress caused by mismatching of the ribbon curvatures, B–H loop appears to be a round type. However, core losses are as low as those of Fe-based amorphous alloys.

A medium-sized toroidal core assembled with this nanocrystalline alloy ribbon, which was secondarily annealed under a perpendicular magnetic field, exhibits core loss at 0.2 T and at 10 kHz of 2 W/kg. This value of core loss is one of the lowest among the metallic cores, which have higher B_s than 1.5 T.

The nanocrystalline material utilized exhibits a high saturation magnetic flux density of 1.74 T and one half of the saturation magetostriction λ_s of Fe-based amorphous alloys with comparable core losses, finding its applications in distribution transformers and power electronics devices.

References

[1] N. P. Goss, "New development in electrolytic strip steels characterized by fine grain structure approaching properties of a single crystal," *Trans. Amer. Soc. Metals*, vol. 23, pp. 515–531, 1935.

[2] G. Y. Chin and J. H. Wernick, *Ferromagnetic Materials*. Amsterdam, The Netherlands: North Holland, 1980.

[3] D. F. Binns, A. B. Crompton, and A. Jaberansari, "Economic design of a 50 kVA distribution transformer. Part 2: Effect of different core steels and loss capitalisations," *IEE Proc. C-Generat., Transmiss. Distrib.*, vol. 133, no. 7, pp. 451–456, 1986.

[4] M. Abe, Y. Takada, T. Murakami, Y. Tanaka, and Y. Mihara, "Magnetic properties of commercially produced Fe-6.5wt% Si sheet," *J. Mater. Eng.*, vol. 11, no. 1, pp. 109–116, 1989.

[5] F. E. Luborsky, *Ferromagnetic Materials*. Amsterdam, The Netherlands: North Holland, 1980.

[6] J. A. Vaccari, "Metallic glass on the way" *Design Eng.*, vol. 52, p. 53–54, Mar. 1981.

[7] Y. Ogawa, M. Naoe, Y. Yoshizawa, and R. Hasegawa, "Magnetic properties of high B_s Fe-based amorphous material," *J. Magn. Magn. Mater.*, vol. 304, no. 2, pp. e675–e677, 2006.

[8] Y. Yoshizawa, S. Oguma, and K. Yamauchi, "New Fe-based soft magnetic alloys composed of ultrafine grain structure," *J. Appl. Phys.*, vol. 64, no. 10, p. 6044, 1988.

[9] Y. Yoshizawa, "Magnetic properties and applications of nanostructured soft magnetic materials," *Scripta Mater.*, vol. 44, nos. 8–9, pp. 1321–1325, 2001.

[10] K. Suzuki, N. Kataoka, A. Inoue, A. Makino, and T. Masumoto, "High saturation magnetization and soft magnetic properties of bcc Fe–Zr–B alloys with ultrafine grain structure," *Mater. Trans. JIM*, vol. 31, no. 8, pp. 743–746, 1990.

[11] M. Yu and Y. Kakehashi, "Existence of the spin-glass state in amorphous Fe," *Phys. Rev. B*, vol. 49, p. 15723, Jun. 1994.

[12] M. Ohta and Y. Yoshizawa, "New high-B_s Fe-based nanocrystalline soft magnetic alloys," *Jpn. J. Appl. Phys.*, vol. 46, nos. 20–24, p. L477, 2007.

[13] M. Ohta and Y. Yoshizawa, "Magnetic properties of nanocrystalline $Fe_{82.65}Cu_{1.35}Si_xB_{16-x}$ alloys ($x = 0$–7)," *Appl. Phys. Lett.*, 91, no. 6, p. 062517, 2007.

[14] M. Ohta and Y. Yoshizawa, "Recent progress in high B_s Fe-based nanocrystalline soft magnetic alloys," *J. Phys. D, Appl. Phys.*, vol. 44, no. 6, p. 064004, 2011.

[15] M. Ohta and Y. Yoshizawa, "High B_s nanocrystalline $Fe_{84-x-y}Cu_xNb_ySi_4B_{12}$ alloys ($x = 0.0$–1.4, $y = 0.0$–2.5)," *J. Magn. Magn. Mater.*, vol. 321, pp. 2220–2224, Jul. 2009.

[16] M. Ohta and Y. Yoshizawa, "Effect of heating rate on soft magnetic properties in nanocrystalline $Fe_{80.5}Cu_{1.5}Si_4B_{14}$ and $Fe_{82}Cu_1Nb_1Si_4B_{12}$ alloys," *Appl. Phys. Exp.*, vol. 2, no. 2, p. 023005, 2009.

[17] A. Makino, H. Men, T. Kubota, K. Yubuta, and A. Inoue, "New Fe-metalloids based nanocrystalline alloys with high B_s of 1.9T and excellent magnetic softness," *J. Appl. Phys.*, vol. 105, no. 7, p. 07A308, 2009.

[18] (2013). *ORIENTCORE*. [Online]. Available: http://www.nssmc.com

[19] (2015). *Super Core*. [Online]. Available: http://www.jfe-steel.co.jp/en/